One-Step Flame-Synthesis of Carbon-Embedded and -Supported Platinum Clusters

Frank O. Ernst, Robert Büchel, Reto Strobel, and Sotiris E. Pratsinis*

Particle Technology Laboratory, Institute of Process Engineering, Department of Mechanical and Process Engineering, ETH Zurich, Sonneggstrasse 3, ML F13, CH-8092 Zurich, Switzerland

Received July 26, 2007. Revised Manuscript Received December 18, 2007

Carbon-embedded or -supported platinum clusters (1−12 wt % Pt) were made rapidly by a scalable, single-step flame spray pyrolysis (FSP) process. Pt-containing precursors dissolved in xylene were sprayed and combusted in a controlled oxidation atmosphere resulting in nanostructured, carbon-embedded Pt clusters. Reversing the order of particle formation by combusting xylene alone and the Pt precursor downstream onto the freshly made carbon particles led to carbon-supported Pt clusters. Both carbon-embedded and -supported Pt clusters possessed the self-preserving size distribution of aerosols grown by coagulation in the free-molecular regime. This indicates a homogeneous gas-phase formation pathway rather than the heterogeneous one typically observed in flame synthesis of noble metal catalysts on ceramic supports. These Pt/C composites were tested as catalysts and characterized by scanning and high-resolution transmission electron microscopy, Raman spectroscopy, nitrogen adsorption, X-ray diffraction, and CO chemisorption. Specific surface areas ranged from 25 to 200 m^2/g and Pt clusters were well-dispersed. Carbon-embedded Pt clusters (2–5 nm) were not accessible for CO chemisorption and inactive as catalysts for hydrogenation of cyclohexene indicating hermetic carbon coating of platinum clusters. In contrast, carbon-supported Pt clusters (5–15 nm) chemisorbed CO and were active hydrogenation catalysts demonstrating the accessibility of their Pt surface.

Introduction

Activated carbon and recently carbon nanotubes are frequently used as noble metal catalyst–supports since they are stable in both acid and basic media. In addition, carbon can be burnt off, allowing for an economic and ecologic recovery of the precious metals.[1] The electronic conductivity of carbon makes it a standard catalytic support material in fuel cell electrodes.[2] Furthermore, supported noble metal catalysts are used for hydrogenation, oxidation, reforming,[3] and other reactions. For their preparation, multistep processes are applied including carbon support generation (generally in a flame) and subsequent loading with noble metals by various wet chemistry methods such as impregnation, precipitation, and others as reviewed recently.[4–7] On the other hand, carbon-embedded Pt clusters are used in sensors for detection of hydrogen peroxide[8] and biomolecules such as glucose, acetylcholine, and choline.[9] They are also applied as electrodes for electroanalysis of hydrogen evolution and dioxygen reduction.[10] For these applications, Pt cluster detachment has to be prevented and thus Pt-clusters are embedded in a carbon matrix. McCreery and co-workers[11] made such materials in glassy carbon by incorporating Pt into carbon precursors and pyrolyzing them at 600 °C. You et al.[10] used a co-sputtering method to embed Pt clusters in graphitelike carbon, whereas Walter et al.[12] report a sonochemical approach to encapsulate Pt nanoparticles into a graphite lattice.

The above studies indicate the applications of Pt clusters either embedded in or supported on carbon matrices. At the same time, it is apparent that their synthesis relies on techniques that involve many process steps and/or are difficult to scale-up to high production rates. Flame technology may offer an alternative route for synthesis of these Pt/C particles as it is used for large scale (tons/h) production of carbon black, fumed silica, alumina and titania pigments[13] and can produce high-purity materials (e.g., optical fibers) with unique (filamentary) morphology and (metastable) phase composition.[14] In fact, carbon-coated titania[15] and silica[16]

* Corresponding author. Phone: 41 44 632 3180. E-mail: pratsinis@ptl.mavt.ethz.ch.

(1) Rodriguez-Reinoso, F. *Carbon* **1998**, *36*, 159–175.
(2) Thompsett, D. Catalysts for Proton Exchange Membrane Fuel Cell. In *Fuel Cell Technology Handbook*, Hoogers, G., Ed.; CRC Press: Boca Raton, FL, 2003.
(3) Ertl, G.; Knözinger, H.; Weitkamp, J. *Handbook of Heterogeneous Catalysis*; VCH/Wiley: Weinheim, Germany, 1997.
(4) Antolini, E. *Mater. Chem. Phys.* **2003**, *78*, 563–573.
(5) Chan, K. Y.; Ding, J.; Ren, J. W.; Cheng, S. A.; Tsang, K. Y. *J. Mater. Chem.* **2004**, *14*, 505–516.
(6) Liu, H. S.; Song, C. J.; Zhang, L.; Zhang, J. J.; Wang, H. J.; Wilkinson, D. P. *J. Power Sources* **2006**, *155*, 95–110.
(7) Zhang, Y.; Erkey, C. *J. Supercrit. Fluids* **2006**, *38*, 252–267.
(8) Ferapontova, E. E.; Grigorenko, V. G.; Egorov, A. M.; Borchers, T.; Ruzgas, T.; Gorton, L. *Biosens. Bioelectron.* **2001**, *16*, 147–157.
(9) You, T. Y.; Niwa, O.; Tomita, M.; Hirono, S. *Anal. Chem.* **2003**, *75*, 2080–2085.
(10) You, T.; Niwa, O.; Horiuchi, T.; Tomita, M.; Iwasaki, Y.; Ueno, Y.; Hirono, S. *Chem. Mater.* **2002**, *14*, 4796–4799.
(11) Callstrom, M. R.; Neenan, T. X.; McCreery, R. L.; Alsmeyer, D. C. *J. Am. Chem. Soc.* **1990**, *112*, 4954–4956.
(12) Walter, J.; Nishioka, M.; Hara, S. *Chem. Mater.* **2001**, *13*, 1828–1833.
(13) Swihart, M. T. *Curr. Opin. Colloid Interface Sci.* **2003**, *8*, 127–133.
(14) Strobel, R.; Pratsinis, S. E. *J. Mater. Chem.* **2007**, *17*, 4743–4756.
(15) Kammler, H. K.; Pratsinis, S. E. *J. Mater. Res.* **2003**, *18*, 2670–2676.

10.1021/cm702023n CCC: $40.75
Published on Web 02/27/2008

nanoparticles have been made already in laboratory- and pilot-scale vapor-fed flames up to 700 g/h by co-oxidation of hydrocarbon and Ti- or Si-organometallic or -chloride precursors. These flames, however, are limited for synthesis of particles with selected component distribution as carbon always ends up on the particle surface as the ceramic support precipitates first from the gas phase and carbon forms on it by surface growth.[15] Flame spray pyrolysis (FSP) offers the possibility of using nonvolatile precursors for synthesis of broad particle compositions and morphologies that have been applied in particular as catalysts[17] as well as for sensors, phosphors, fuel cells, dental and bone nanocomposites, and even for nutritional supplements.[14] Furthermore, multiple FSP units can be used for selected component distribution within particles as has been shown recently in synthesis of active $Pt/Ba/Al_2O_3$ catalysts for nitrogen storage reduction by promoting component mixing at the nano rather than at the atomic level.[18]

Here, the potential of flame technology for synthesis of Pt/C particles with selected component distribution is explored, for the first time to the best of our knowledge. This is challenging as Pt catalyzes the combustion of carbon.[19] It is therefore not trivial to form Pt/C by co-oxidation of appropriate precursors as with standard FSP-made Pt/ceramic nanoparticles.[20] So an FSP process is developed to allow for substoichiometric combustion of xylene aerosol and controlled formation of carbon. Adding a Pt-precursor to xylene followed by their partial co-oxidation leads to carbon embedded Pt clusters while separately spraying and combusting of the Pt precursor and mixing its plume downstream with the soot-laden gases xylene FSP leads to Pt clusters supported on carbon. In both cases, Pt/C particles are produced in a scalable, one-step gas phase process. The Pt cluster size distributions are counted revealing a homogeneous aerosol formation pathway in contrast to the heterogeneous one which is known for noble metal clusters on ceramic supports made by conventional FSP. Finally, physical and catalytic properties of the Pt/C particles are evaluated and compared to literature.

Experimental Section

Particle Synthesis. Figure 1 shows the experimental setup for synthesis of carbon-embedded and -supported Pt clusters by FSP.[21] Xylene (Riedel-de Haën, >96%) was fed into the nozzle (of FSP1) by a syringe pump (Inotech R232) at 2.2–5 mL/min and dispersed by 3–5 L/min nitrogen (Pan Gas, >99.95%) into fine droplets. The spray was ignited and maintained by a premixed flame ring surrounding the spray capillary.[21] This premixed methane/oxygen supporting flame ring was fed by 1.63 L/min CH_4 and 3.88 L/min O_2 throughout all experiments. The reactor is surrounded by a 50 mm outer diameter and 400 mm long quartz glass tube (wall thickness 2 mm). Oxygen and nitrogen were fed as sheath gas with a constant total flow of 7 L/min through a sinter metal ring (8 mm width and 9 mm inner diameter) surrounding the supporting flame.[21] The stoichiometry during combustion was controlled by varying the sheath nitrogen to oxygen ratio from 0 to 1.33. Gas flows were monitored by calibrated mass flow controllers (Bronkhorst). With the aid of a vacuum pump, product particles were collected on a glass fiber filter (GF/D Whatman, 257 mm in diameter). During particle synthesis, the quartz glass tube was coated progressively with soot, inhibiting direct flame diagnostics.

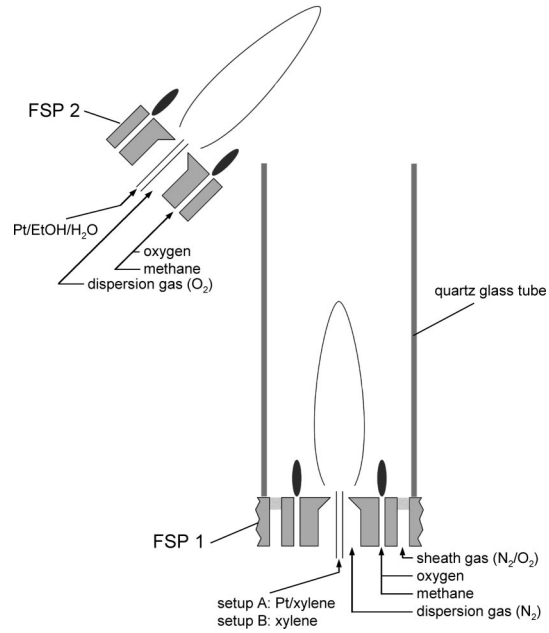

Figure 1. Experimental setup consists of a flame spray pyrolysis (FSP) unit with a reaction chamber (chimney) enclosed by a quartz glass tube, FSP1. C-embedded Pt clusters were made by dissolving Pt-precursor in xylene and co-oxidizing them. An additional FSP unit (FSP2) was used for synthesis of C-supported Pt clusters. The Pt precursor was dissolved in ethanol/water solution, sprayed, and combusted through the FSP2 unit at the top of the FSP1 chimney into the carbon-loaded effluents of FSP1.

For synthesis of carbon-embedded Pt clusters, platinum acetylacetonate ($Pt(acac)_2$, Strem Chemicals, 98%) was dissolved in xylene and simultaneously fed into the flame, referred to as setup A in Figure 1 (only FSP1 operated). The $Pt(acac)_2$ precursor concentrations were chosen as to result in 1 to 5 wt % Pt loading of the final product, whereas the total precursor flow rate was in the range from 2.2 to 5 mL/min.

For synthesis of carbon-supported Pt clusters, FSP1 (Figure 1) was used as carbon source while a second FSP unit (FSP2) delivering the Pt precursor was at the top end of the quartz glass tube at an angle of 45° (setup B). In FSP2 (same flow rates applied as described above unless otherwise indicated), oxygen was used as dispersion gas at 3 L/min while the liquid precursor consisted of a mixture of ethanol (Fluka), water (deionized), and $Pt(acac)_2$. The ethanol (EtOH) fraction in the $EtOH/H_2O$ solvent was varied from 0.5 to 1.0 and $Pt(acac)_2$ concentrations were adjusted to obtain 2.7 to 12 wt % Pt in the product powder.

Flame conditions were characterized by the (overall) equivalence ratio (EQR), Φ, of the reactants averaged over the entire flame[22]

(16) Kammler, H. K.; Mueller, R.; Senn, O.; Pratsinis, S. E. *AIChE J.* **2001**, *47*, 1533–1543.
(17) Strobel, R.; Baiker, A.; Pratsinis, S. E. *Adv. Powder. Technol.* **2006**, *17*, 457–480.
(18) Strobel, R.; Madler, L.; Piacentini, M.; Maciejewski, M.; Baiker, A.; Pratsinis, S. E. *Chem. Mater.* **2006**, *18*, 2532–2537.
(19) Stein, H. J. *Appl. Catal., B* **1996**, *10*, 69–82.
(20) Strobel, R.; Stark, W. J.; Madler, L.; Pratsinis, S. E.; Baiker, A. *J. Catal.* **2003**, *213*, 296–304.
(21) Mädler, L.; Kammler, H. K.; Mueller, R.; Pratsinis, S. E. *J. Aerosol Sci.* **2002**, *33*, 369–389.
(22) Turns, S. A. *An Introduction to Combustion; Concepts and Applications*; McGraw-Hill: New York, 1996.

$$\Phi = \frac{(n_{\text{fuel}}/n_{\text{oxidant}})_{\text{real}}}{(n_{\text{fuel}}/n_{\text{oxidant}})_{\text{stoichiometric}}}, \quad (1)$$

where n is the average molar concentration. The influence of EQR changes by the addition of Pt precursor were neglected as its contribution to the calculated stoichiometry was less than 0.2%.

To determine the yield, the collected particles on the filter were heated for 1 h at 110 °C and 0.66 atm (absolute) to ensure desorption of water and unburnt residuals (such as xylene). The carbon yield, χ_c, was calculated according to

$$\chi_c = \frac{m_{\text{filter}}\,(1 - c_{\text{Pt}})}{m_c} \quad (2)$$

where m_{filter} is the product particle mass collected on the filter during particle synthesis (accuracy ± 2 mg), m_c is the total mass of carbon available in the precursor liquid solution, and c_{Pt} is the Pt concentration of the product powder.

Powder Characterization. The Brunauer–Emmett–Teller (BET)-equivalent specific surface area (SSA) of the powder was determined from a 5-point nitrogen adsorption isotherm at 77 K in the relative pressure range $p/p_0 = 0.05$ to 0.25 (Tristar, Micromeritics Instruments Corp.). All samples were degassed in N_2 at 150 °C for 1 h prior to analysis. The crystallite sizes, $d_{\text{Pt,XRD}}$, of the Pt-clusters were determined from X-ray diffraction (XRD) patterns recorded with a Bruker AXS D8 Advance (40 kV, 40 mA, $\lambda = 1.54$ nm) at a scan speed of 0.5°/min and $10° < 2\theta < 70°$ based on the fundamental parameter approach and the Rietveld method[23] with TOPAS2 software.

Samples were dispersed in ethanol and deposited onto a perforated carbon foil supported on a copper grid (Okenshoji Co., Ltd.) for transmission electron microscopy (TEM) performed on a CM30 (FEI; LaB6, operated at 300 kV). High-resolution TEM (HRTEM) images were recorded with a slow-scan CCD camera. Scanning transmission electron microscopy (STEM) images, obtained with a high-angle annular dark-field (HAADF) detector attached to the Tecnai 30F microscope (FEI, field emission cathode, operated at 300 kV), show the metal particles with bright contrast (Z contrast).

The actual Pt-loading was measured thermogravimetrically, by burning the carbon support in an oxidizing atmosphere with a Mettler Toledo TGA/SDTA851^e thermobalance. About 100 mg samples in an alumina crucible were heated at a rate of 10 °C/min to 600 °C and there for 1 h in air. All Pt loadings in this paper are actual loadings and have been determined thermogravimetrically.

Platinum dispersions were determined by CO-pulse chemisorption at 40 °C with 50 mL/min He and pulses of 0.5 mL (10% CO in He) on a Micromeritics Autochem II 2920 unit. Prior to dispersion analysis all samples were freshly reduced for 30 min at 350 °C under flowing hydrogen (20 mL/min) and then flushed by He (50 mL/min) at that temperature for 30 min. To calculate the metal dispersion, an adsorption stoichiometry of Pt/CO = 1 was assumed.[24]

Hydrogenation of cyclohexene was used to test the catalytic activity of Pt/C particles in a magnetically stirred 50 mL glass reactor. In the standard procedure, 10 mg of Pt/C catalyst in 10 mL of methanol (Fluka, 99.8%) were first pretreated in situ under flowing hydrogen (99.5%, PanGas, 50 mL/min) for 5 min at 1 bar and 0 °C. The reaction started by adding 1 mL of cyclohexene (Fluka) under 1 bar H_2. The conversion was determined by gas chromatography (ThermoQuest TraceGC equipped with an FID detector and a Zebron ZB624 column) of samples extracted at various times. As reference, 5 wt-% Pt on activated carbon (Aldrich) was used.

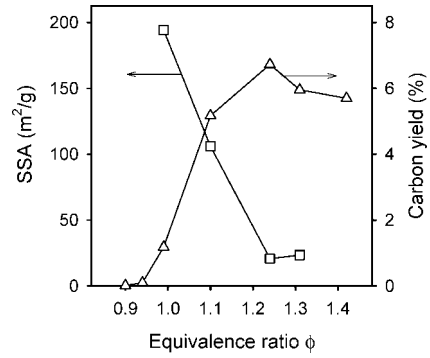

Figure 2. Carbon black yield (eq 2) and SSA as function of equivalence ratio (Φ, eq 1) in the absence of Pt. A minimum temperature is reached at maximum carbon yield and the SSA reached a maximum for stoichiometric combustion.

Results and Discussion

Carbon Black. First, carbon black formation by combustion of xylene, using only FSP1 (Figure 1) with no Pt being present, was investigated by monitoring its specific surface area and yield as a function of equivalence ratio, Φ. The carbon yield reaches a maximum for $\Phi \approx 1.23$ resulting in a production rate of 18 g/h. Increasing Φ less oxygen is available for combustion and thus less soot is formed as not all xylene is converted. For $\Phi < 1.23$ most of the xylene is oxidized to CO/CO_2 and H_2O thus carbon black formation is low. At $\Phi = 0.9$, the collected carbon black was too little for SSA analysis placing a lower limit for the process. A maximum SSA of 194 m^2/g was observed around stoichiometric combustion ($\Phi = 1$). This is in agreement with other studies where a linear decrease of the SSA with increasing fuel-to-air ratio was reported.[25] Comparing SSA and yield shows that powder with high SSA can be produced at low yields only: the SSA drops below 20 m^2/g at the maximum yield. At $\Phi > 1$, few but large carbon particles are formed resulting in lower SSA. Increasing carbon yield caused increased carbon concentration in the flame which in turn results in large particles or agglomerates (with low SSA). This is in agreement with particle formation models in flames[26] as collision probabilities are a function of C-concentration squared. Raman analysis (not shown) of carbon black samples with SSAs of 194, 40, and 36 m^2/g produced at $\Phi = 1.08$, 1.13, and 1.38, respectively, revealed well-pronounced G (around 1582 1/cm) and D (around 1357 1/cm) bands that are typical for carbon black.[27]

Pt Clusters Embedded in Carbon. Two conditions for carbon black synthesis were chosen to analyze formation of carbon-embedded Pt-clusters using only FSP1 (Figure 1). At $\Phi = 1.31$ and 1.10 the yield is high and the SSAs are 25 and 105 m^2/g, respectively (Figure 2). Different Pt-contents in the final product (1 to 5 wt-%) were achieved by controlling the $Pt(acac)_2$ concentration in xylene.

(23) Cheary, R. W.; Coelho, A. A. *J. Appl. Crystallogr.* **1998**, *31*, 851–861.
(24) Freel, J. *J. Catal.* **1972**, *25*, 149–160.
(25) Chughtai, A. R.; Kim, J. M.; Smith, D. M. *J. Atmos. Chem.* **2002**, *43*, 21–43.
(26) Smith, O. I. *Prog. Energy Combust. Sci.* **1981**, *7*, 275–291.
(27) Jawhari, T.; Roid, A.; Casado, J. *Carbon* **1995**, *33*, 1561–1565.

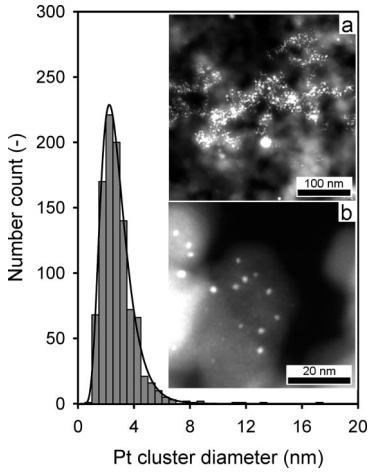

Figure 3. (a, b) STEM images of carbon embedded Pt-clusters synthesized at $\Phi = 1.10$ in FSP1 and a Pt loading of 2.6 wt %. Single Pt clusters in the size range of tens of nanometers and well-distributed smaller (around 2 nm) Pt clusters are observed. The particle size distribution was extracted by counting ($n = 1002$) from Figure 3a. The count mean diameter is 2.6 nm and the geometric standard deviation is 1.46 corresponding to aerosol formation by coagulation in the free-molecular regime.[29,30]

Figure 3 shows STEM images of 3.0 wt-% Pt embedded in carbon made at $\Phi = 1.31$. The Pt clusters seem well-dispersed; however, Figure 3a shows few single Pt clusters in the size range of tens of nanometers. This is attributed to incomplete Pt precursor droplet evaporation at short residence time at high temperatures.[28] At higher magnification (Figure 3b), a distribution of much smaller narrowly distributed Pt clusters (about 2 nm) was detected also. Increasing the Pt content (not shown) also increased Pt cluster size as expected by coagulation and condensation.[29] The Pt cluster size distribution (Figure 3) was extracted by counting ($n = 1002$) particles as in Figure 3a. The count mean diameter is 2.6 nm and the geometric standard deviation of $\Sigma_g = 1.46$ corresponds well to the theoretical value of 1.46 for aerosol formation by coagulation in the free-molecular regime.[30] This indicates a gas-phase formation pathway for Pt clusters that is quite different than the heterogeneous route of their formation on ceramic supports by FSP.[20] Once these Pt clusters are formed, graphitic-like carbon forms on them by surface growth similar to silica[16] or titania.[15]

Figure 4 shows XRD analyses for high SSA (105 m^2/g) carbon black ($\Phi = 1.10$) with various Pt loadings. For Pt loadings below 1.1 wt %, no Pt crystallites could be detected by XRD indicating very small clusters whereas a small Pt^0 peak ($2\theta = 39°$) could be observed for 1.4 wt % Pt. This is in agreement with earlier studies[20] reporting no Pt detection when having small noble metal particles of low concentration on alumina supports. The detected crystallite size increased with increasing Pt-loading from $d_{Pt,XRD} = 13.2$ nm (1.4 wt % Pt) to 16.4 nm (2.6 wt % Pt) and 17.9 nm (5.0 wt % Pt). This is expected from coagulation theory for increasing metal concentration[29] in the flame. Though the power of the

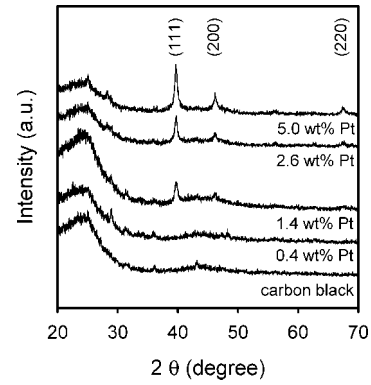

Figure 4. XRD patterns for Pt/C particles at various Pt loadings synthesized at $\Phi = 1.10$ in FSP1. Only at Pt loadings above 1 wt % crystalline Pt^0 could be detected.

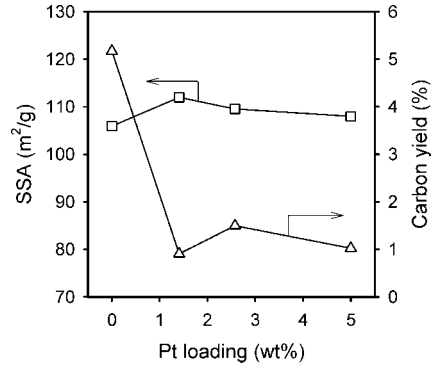

Figure 5. SSA and carbon yield as function of Pt loading synthesized at $\Phi = 1.10$ in FSP1. The presence of Pt lowered the carbon yield by 80% through catalytic burnoff.

concentration dependence of the final particle diameter (about 0.25) is below the theoretical value of 0.4 for coagulation,[31] this is distinctly different from cluster formation on inorganic supports that does not follow coagulation theory but rather heterogeneous processes as has been shown for gold clusters on the surface of SiO_2 or TiO_2.[31] This indicates again that Pt clusters form independently of the carbon matrix.

The Pt loading of the product depends not only on the Pt content in the precursor but also on the carbon yield. If the latter is reduced, the product Pt-loading increases without changing the Pt concentration in the precursor. Figure 5 shows SSA and carbon yield as function of Pt loading of the product powder for the conditions of Figure 4 ($\Phi = 1.10$). The presence of Pt had only little influence on the product SSA and generally reduced the carbon black yield by a factor of 5 resulting in a production rate of 3 g/h. This can be attributed to the catalytic activity of Pt that accelerates carbon combustion. This catalytic effect is also used in car industry to burn off undesired soot emissions.[19] The SSA of the Pt/C samples was about 105 m^2/g and the corresponding carbon yield was essentially independent of the product Pt-loading. This indicates that for catalytic combustion of carbon, the number of Pt surface sites is not the limiting step, at least, in the range of 1.4−5 wt % Pt.

Figure 6 shows a representative HR-TEM image of the particles in images a and b of Figure 3. Two Pt clusters, as detected from their crystal lattices, are coated by carbon

(28) Schulz, H.; Madler, L.; Strobel, R.; Jossen, R.; Pratsinis, S. E.; Johannessen, T. *J. Mater. Res.* **2005**, *20*, 2568–2577.
(29) Friedlander, S. K. *Smoke, Dust, and Haze: Fundamentals of Aerosol Dynamics*; Oxford University Press: New York, 2000.
(30) Landgrebe, J. D.; Pratsinis, S. E. *Ind. Eng. Chem. Res.* **1989**, *28*, 1474–1481.
(31) Koch, W.; Friedlander, S. K. *Part. Part. Syst. Charact.* **1991**, *8*, 86–89.

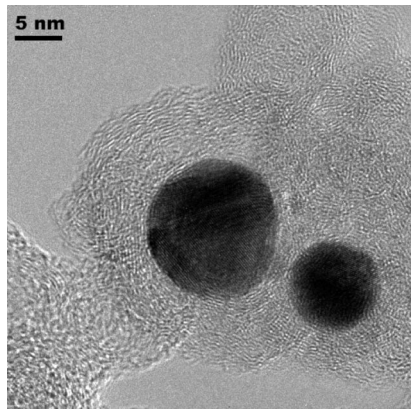

Figure 6. HR-TEM image of carbon-embedded Pt-clusters synthesized at $\Phi = 1.10$ in FSP1. Pt clusters are surrounded by layered carbon. The Pt clusters serve as nucleation sites for the carbon indicating the sequential formation of Pt nuclei followed by surface growth of carbon.

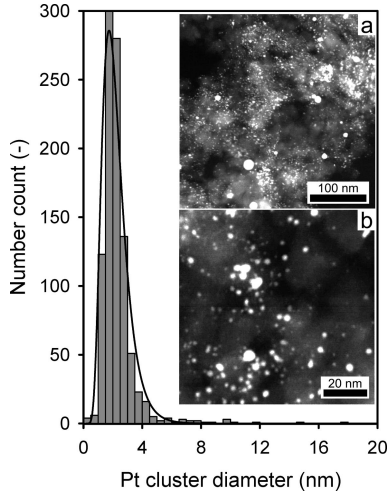

Figure 7. STEM image of carbon-supported Pt clusters synthesized at $\Phi = 1.31$ and pure ethanol as solvent for the Pt precursor feed through FSP2 resulting in 12 wt % Pt. Few single Pt clusters in the size range of several tens of nanometers and well-distributed smaller 5–15 nm Pt clusters were observed. The particle size distribution was extracted by counting ($n = 998$) from Figure 7a. The count mean diameter is 2.1 nm and the geometric standard deviation is 1.47 corresponding to aerosol formation by coagulation in the free-molecular regime[29,30] indicating that Pt cluster formation takes place in the gas phase and then deposit onto the available carbon surface.

layers. The Pt clusters seem to serve as nucleation sites for the carbon to grow layer-wise on their surfaces (surface growth). No chemisorption of CO on Pt could be observed for all samples synthesized using only FSP1. Together with the inactivity of these samples for catalytic hydrogenation of cyclohexene, this indicates complete or hermetic coating of all Pt clusters with carbon.

Carbon-Supported Pt Clusters. FSP1 and FSP2 (Figure 1) were used for flame-synthesis of carbon-supported Pt clusters by reversing the order of carbon and Pt formation. This was accomplished by using FSP1 as carbon particle source at $\Phi = 1.31$ and introducing Pt further downstream by FSP2 (Figure 1). The influence of Pt addition was investigated by changing the combustion enthalpy density (EtOH fraction from 0.5 to 1.0 in the EtOH /water solvent) of its precursor solution fed through FSP2. Figure 7 shows two magnifications of STEM images of Pt/C samples made with pure ethanol solvent (in FSP 2) resulting in Pt (12 wt %) that seems to be well dispersed in the product powder. Again, few larger Pt clusters are visible that may result from incomplete droplet evaporation as discussed before and becomes even more pronounced when reducing the combustion enthalpy and therefore the flame temperature of FSP2. The particle size distribution (Figure 7) was extracted by counting ($n = 998$ particles) from Figure 7a. The count mean diameter is 2.1 nm and the geometric standard deviation is 1.47 corresponding again well to the 1.46 value for aerosol formation by particle coagulation in the free-molecular regime.[30] This indicates that Pt-clusters were formed homogeneously in the gas-phase by nucleation and coagulation in the free molecular regime and subsequently deposited onto the available carbon surface. This formation pathway is different than that of flame-made noble metal clusters on ceramic supports where such clusters are formed heterogeneously on the ceramic support.[32]

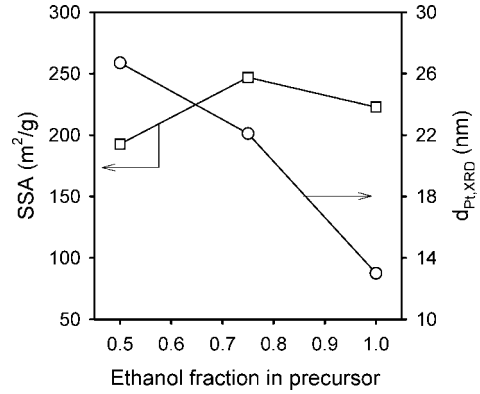

Figure 8. SSA and Pt crystallite size ($d_{Pt,XRD}$) as a function of precursor (FSP2) ethanol fraction at $\Phi = 1.31$. Lower ethanol fractions decreased the FSP2 flame temperature and led to larger Pt clusters by incomplete droplet evaporation.

Figure 8 shows the SSA and Pt cluster crystallite size, $d_{Pt,XRD}$, as a function of EtOH fraction in the precursor FSP2 solvent. The SSA of about 220 m^2/g was hardly affected by the EtOH fraction, though it is much higher than that (25 m^2/g for $\Phi = 1.31$ in Figure 2) without the FSP2 flame. This could be attributed to carbon burnoff[33] either thermally in the second flame (FSP2) or catalytically by the presence of Pt-clusters in the mixed plume of FSP1 and FSP2. The somewhat lower SSA for an EtOH fraction of 0.5 may be reasoned by the lower flame enthalpy density and subsequently lower temperature resulting from the FSP2 precursor solution composition. Lowering the temperature (by using lower ethanol fractions) may have led to incomplete combustion and dissociation of the Pt precursor as also indicated by the increased crystallite sizes, $d_{Pt,XRD}$. This is supported by the lack of CO-adsorption (Table 1) and catalytic activity for this powder (as discussed further down). Only little, if any, Pt surface seemed to be available, in agreement with the increased $d_{Pt,XRD}$.

The Pt dispersion as extracted from CO-chemisorption is listed in Table 1 for the sequence of powders described in

(32) Madler, L.; Stark, W. J.; Pratsinis, S. E. *J. Mater. Res.* **2003**, *18*, 115–120.
(33) Spicer, P. T.; Artelt, C.; Sanders, S.; Pratsinis, S. E. *J. Aerosol Sci.* **1998**, *29*, 647–659.

Table 1. Pt Content and Dispersion, Turnover Frequency, and Ethanol Fraction (of the FSP2 ethanol/water solvent) of FSP-Made Pt Clusters Supported on or Embedded in Carbon

	EtOH fraction in FSP2 solvent	Pt loading of product powder (wt %)	Pt dispersion (%)	TOF (s^{-1})
C-supported Pt clusters	1.0	12	14	4.05
	reference (Aldrich)	5	17	4.18
	0.75	10	5	4.38
	0.5	3	<1	
C-embedded Pt clusters		2.6	<1	

Figure 8 indicating active and available Pt surface for EtOH fractions larger than 0.5. Figure 9 shows a typical HR-TEM image of these Pt/C particles made with pure ethanol as solvent for the Pt-precursor in FSP2. In contrast to carbon-embedded Pt clusters (Figure 6), well-developed Pt clusters are located on the carbon surface. They are well-attached to it with a good fraction of Pt surface exposed for reaction.

Figure 10 depicts the conversion of cyclohexene to cyclohexane using flame-made carbon-embedded and -supported Pt clusters. All carbon-embedded Pt materials were inactive and no conversion of cyclohexene was observed as exemplarily shown for the material of Figure 6 (diamonds). In agreement with CO-chemisorption (Table 1), this can be attributed to the complete coverage of the active Pt surface

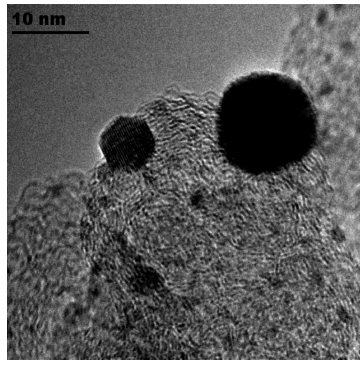

Figure 9. HR-TEM image of carbon-supported Pt clusters synthesized at $\Phi = 1.31$ and 12 wt % Pt loading. In contrast to carbon-embedded Pt clusters, well-developed Pt clusters are well-attached on the carbon surface with parts of their surface accessible for reaction.

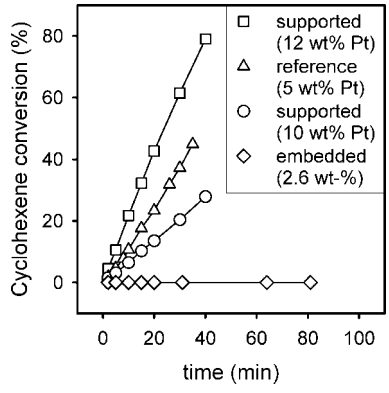

Figure 10. Catalytic hydrogenation of cyclohexene: conversion as function of time. Carbon-embedded Pt clusters showed no activity, whereas higher Pt loadings led to increased activity for carbon-supported Pt clusters. The reference sample ranged in between, because of its smaller Pt cluster size.

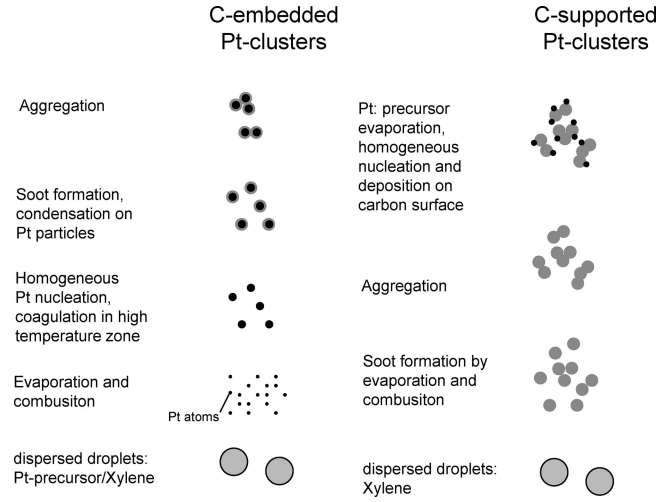

Figure 11. Synthesis pathways of carbon-embedded and carbon-supported Pt clusters. For the former, Pt clusters serve as nucleation sites for the carbon matrix, whereas for the latter, Pt attaches on previously formed carbon particles (nanoscale mixing).

by carbon not leaving any Pt surface accessible for hydrogenation as reactants cannot diffuse through the carbon layer. In contrast, carbon-supported Pt materials were catalytically active for hydrogenation of cyclohexene as shown in Figure 10 for Pt loadings of 10 and 12 wt % corresponding to EtOH fractions of 0.75 (circles in Figure 8) and 1.0 (squares) in the FSP2 precursor solvent. Pt clusters are on the carbon surface and the Pt surface is accessible for catalysis (Figure 9). The reference sample with 5 wt % Pt on activated carbon (triangles) showed an activity between the two flame-made C-supported samples. This may be explained by its higher Pt dispersion (Table 1) and therefore smaller Pt-cluster size. Taking into account the dispersion and relating the moles of cyclohexene converted per mole surface Pt as a function of time gives the turnover frequency (TOF). This is about the same for all samples investigated as shown in the last column of Table 1 and indicates that the TOF is only determined by the amount of available Pt and independent of the preparation method. These values, as a measure of catalytic activity, distinguish the presence of carbon-embedded (inactive) or -supported (active) Pt clusters.

Particle Synthesis Pathways. The application of FSP1 and FSP2 as defined in Figure 1 results in different product morphologies as analyzed above. Figure 11 depicts the two pathways of particle formation. When using only FSP1, the combined Pt and carbon precursor is dispersed into droplets, evaporated and combusted delivering the energy for the process. Pt clusters nucleate and coagulate in the hot zone of the flame and serve as nuclei for carbon surface growth resulting in coated particles that may then aggregate resulting in the observed carbon-embedded Pt nanoparticles.

Using FSP1 and FSP2, xylene is dispersed into droplets that evaporate and combust substoichiometrically. Soot forms by reaction, surface growth, and aggregation until it reaches the point where Pt precursor is added. Pt-containing precursor is also dispersed into droplets, evaporated and Pt nucleates and coagulates in the gas-phase and deposits onto the available carbon surface. At high temperatures, either by close proximity to the tube outlet or high energy density of

the second flame (high ethanol/water ratio), carbon first burns off leading to high SSA and small Pt clusters. This process results in carbon-supported Pt clusters.

Conclusions

Platinum clusters embedded in or supported on carbon particles can be prepared by a one-step flame technology allowing for mixing of Pt with carbon at the atomic or nano level, respectively. Without Pt being present, the maximum carbon yield was observed at the lowest flame enthalpy density while the highest SSA was obtained close to stoichiometry but was accompanied by a small particle yield.

By introducing the Pt precursor with the xylene fuel, 0.2–5.0 wt % Pt clusters embedded in carbon black were formed. Few large Pt particles were detected by XRD and STEM, the majority, however, though was in the range of 2–5 nm. The presence of Pt decreased the carbon yield by catalytic burnoff. Changing the loading, however, had only little effect. In this process, carbon most likely forms by surface growth heterogeneously on early formed Pt-clusters covering them entirely. This was shown by the inactivity of these materials for hydrogenation of cyclohexene and the absence of Pt surface sites for CO-chemisorption.

Carbon-supported Pt clusters were made by adding Pt downstream of carbon formation with the aid of an additional gas assisted nozzle. Varying the ethanol/water ratio in the solvent through the second nozzle enabled Pt-cluster formation at various temperatures resulting in loadings from 2.7 to 12 wt % and controlled Pt cluster sizes. These carbon-supported Pt clusters exhibited catalytic activity comparable to the literature for hydrogenation of cyclohexene highlighting the potential of flame technology for rapid and scalable synthesis of nanocomposite Pt/C particles. Here, Pt clusters were formed homogeneously in the gas-phase by coagulation in the free molecular regime as indicated by the geometric standard deviation of their measured size distribution. This formation pathway is opposite to that of standard FSP-made noble metal clusters being formed heterogeneously on ceramic supports.

Acknowledgment. We thank Drs. L. Hardwick and P. Novák (Paul-Scherrer-Institute) for the Raman spectroscopy and Dr. F. Krumeich (ETH Zurich) for electron microscopy measurements. Furthermore, we appreciate the electron microscopy center of ETH Zurich (EMEZ) for providing the necessary infrastructure as well as the financial support under ETH Grant TH-29/05-2.

CM702023N